Performance Analysis of a Rotor Flux-Oriented Control in Induction Traction Motor

Tudor Mătușa*, Mihaela Popescu*, Alexandru Bitoleanu* and Constantin Vlad Suru*
* University of Craiova, Faculty of Electrical Engineering, Craiova, Romania, matusa.tudor.e8y@student.ucv.ro
mpopescu@em.ucv.ro, alex.bitoleanu@em.ucv.ro, vsuru@em.ucv.ro

***Abstract* - The superiority of using field-oriented control in electric drive systems based on induction motor has been proven over the years. To increase efficiency, maintainability, reliability and dynamic performance, modern electric traction systems use induction motors. In this context, this paper is focused on the performance determination and analyzing of the rotor flux-oriented control with voltage control, on an induction traction motor, in order to its implementation. First, the control scheme and calculation fundamentals are presented. Then, after the entire system modeling in Simulink environment, the performance of the system in dynamic and steady-state regimes is presented by simulating the operation of a real traction motor at three prescribed speeds. Also, a specific phenomenon of electric locomotives, respectively the passage of wheels over the rail joints is taking into account. To determine the performances, the results obtained from simulating the acceleration process by prescribing a speed ramp, operating in steady-state regime and then electric braking with energy recovery were analyzed. In the paper, three situations are presented: the prescription of a low speed, about 20 % of the nominal speed, of the highest speed, about 160 % of the nominal speed and of three speed steps up to the nominal speed. The analysis of the results leads to the conclusion that there is a very accurate tracking of the prescribed quantities by the actual quantities controlled in the system. It is also highlighted that the peak current through the motor does not exceed its limiting value and the switching frequency of the power electronic devices is lower than the imposed limit value. The analysis of steady-state performance shows that it is also very good.**

Cuvinte cheie: *control orientat după fluxul rotoric, motor cu inducție, sistem de tracțiune, control al vitezei..*

Keywords: *rotor flux-oriented control, induction motor, traction system, speed control.*

I. INTRODUCTION

It is well known that the principle of the field-oriented control proposed by Blaschke [1] starts from the goal of obtaining a behavior of the induction motor similar to that of the DC motor. Explicitly, this means that the torque and the magnetic flux are decoupled. In this way, the magnetic flux and the torque developed by the motor are controlled independently, and the synthesis of the regulators in the structure of the control scheme is more precise, because it operates with quantities whose steady-state values are constant. Most contributions in the literature over time are related to improving performance and also to the implementation of the controls strategies [2]–[20].

The main specific requirements for electric traction systems with induction motors refer to: high power, speed regulation in a wide range (from about 2% to (160-200)% of the nominal frequency), high starting torques, but with a sufficiently low increase in speed, to avoid the phenomenon of slipping, efficient braking with kinetic energy recovery and high reliability.

In order to respond to these requirements and to have a less complicated control, the rotor flux-oriented control is often adopted. It involves working in the (d, q) rotating reference frame, whose d-axis is aligned with the vector of rotor flux. In this way, the control of rotor flux is performed by means of the d-axis stator current of the motor, while the control of the torque is achieved through the q-axis stator current. Moreover, it is allowed to extend the speed variation range well above the nominal speed by weakening the field [4]–[7].

Regarding the type of adopted control (direct or indirect), it is specified that the most frequently used is indirect control [8]-[14]. Thus, the rotor flux and its position angle are calculated using some easily measurable quantities, using the induction motor model and it is not necessary to place sensors in the rotor circuit (as is specific to direct control).

The existence of four controllers (speed controller and active current controller in the first path and, respectively, rotor flux controller and reactive current controller in the second path) is specific to voltage control of the system. Among the modulation strategies adopted in the inverter control, sinusoidal modulation stands out [12], [15], [16].

Among the application areas of the field-oriented control, electric traction is also found [5], [12]–[18].

It should be noted that, in the case of railway traction, the control system must manage the behavior of the system when the wheels pass over the rail joints, so as to minimize the effects that occur. There are very few approaches in the literature on this topic. [19], [20].

This paper deals with the implementation of the rotor flux-oriented control with voltage control on a traction induction motor used in Romanian locomotives. Next, the structure of the paper is as follows. The adopted control scheme and the related calculation bases are the subject of Section II. The MATLAB SIMULINK implementation of the control algorithm is presented in the next section. Then, the performance of the traction system with rotor flux-oriented control is analyzed both in the dynamic regime and in the steady-state regime. Thus, the results obtained from simulating the acceleration process by prescribing a speed ramp, operation in steady-state regime and then electric braking with energy recovery, in three cases are presented, as follows: prescribing of a low speed

(about 20 % of the nominal speed); prescribing speed up to nominal value in three steps and braking in two steps; prescribing of the highest speed (about 160 % of the nominal speed). Finally, some conclusions are formulated.

II. The Control Scheme and Calculation Fundamentals

As illustrated in Fig. 1, there are two cascade control paths in the control system. Also, each o them contains two controllers, so that, there are four controllers.

In the first control path (of the speed and active current), the speed controller (R_ω) provides the prescribed active current (i^*_{sq}) and the active current controller (R_{iq}) provides the quantity u^*_{sq}, which is the prescribed voltage on the q axis of the system synchronous with the rotor flux vector.

In the second control path (of the rotor flux and reactive current), the flux controller (R_ψ) provides the prescribed reactive current (i^*_{sd}), and the reactive current controller (R_{id}) provides the quantity u^*_{sd}, which is the prescribed voltage on the d axis of the system synchronous with the rotor flux vector.

A two-step conversion of the prescribed quantities u^*_{sq} and u^*_{sd} follows. In the first stage (block B1), the conversion is from rotating coordinate system (d, q) to the fixed coordinate system (α, β).

In the second stage (block B2), the conversion is from fixed coordinate system (α, β) to the three-phase system (quantities u^*_a, u^*_b and u^*_c). Then, the sinusoidal modulator (PWM block) performs the synthesis of the control signals for the inverter transistors.

On the feedback path, the three stator currents $i_{sa,b,c}$ measured with current transducers T_i are transformed (in block B3), from the three-phase system (a, b, c) to the fixed coordinate system (α, β) characterised by the components $i_{s\alpha}$ and $i_{s\beta}$. Specific relationships are used for the transformation from one coordinate system to another [20].

As shown in Fig. 1, using the measured currents and the measured speed ω with the speed transducer T_ω, the rotor flux Ψ_r, and its position angle λ between the rotating coordinate system (d, q) and fixed coordinate system (α, β) are calculated in block B4.

The rotor flux components in the fixed coordinate system (α, β) are calculated as follows [20]:

$$\psi_{r\alpha} = \int \left(-p\omega\psi_{r\beta} - \frac{1}{T_r}\psi_{r\alpha} + \frac{L_m}{T_r} i_{s\alpha}\right) dt\,; \quad (1)$$

$$\psi_{r\beta} = \int \left(p\omega\psi_{r\alpha} - \frac{1}{T_r}\psi_{r\beta} + \frac{L_m}{T_r} i_{s\beta}\right) dt; \quad (2)$$

Thus, the calculated rotor flux is expressed as:

$$|\psi_r| = \sqrt{\psi^2_{r\alpha} + \psi^2_{r\beta}}\,; \quad (3)$$

In the above expressions, $T_r = L_r/R_r$, R_r and L_r are the resistance and inductance on a rotor phase referred to the stator, L_m is the magnetization inductance, p is the number of pole pairs, and the angle λ is determined by trigonometric functions [20]:

$$\cos(\lambda) = \frac{\psi_{r\alpha}}{|\psi_r|} = \frac{\psi_{r\alpha}}{\sqrt{\psi^2_{r\alpha}+\psi^2_{r\beta}}}\,; \quad (4)$$

$$\sin(\lambda) = \frac{\psi_{r\beta}}{|\psi_r|} = \frac{\psi_{r\beta}}{\sqrt{\psi^2_{r\alpha}+\psi^2_{r\beta}}}\,; \quad (5)$$

The transformation of the stator currents from the stationary reference frame (α, β) to the rotating reference frame (d, q) is achieved in block B5..

Finally, the sinusoidal modulation principle is implemented in the PWM modulator block, having as inputs the prescribed phase voltages.

III. Matlab-Simulink Implementation of the Control Algorithm

A specific Matlab-Simulink model has been created to determine the dynamic and steady-state performance of the system (Fig. 2). In addition to the main blocks, there are auxiliary blocks used to determine the quantities of interest.

The power part in Fig. 2 consists of the DC source equivalent to the intermediate circuit, the voltage inverter and the squirrel-cage induction motor.

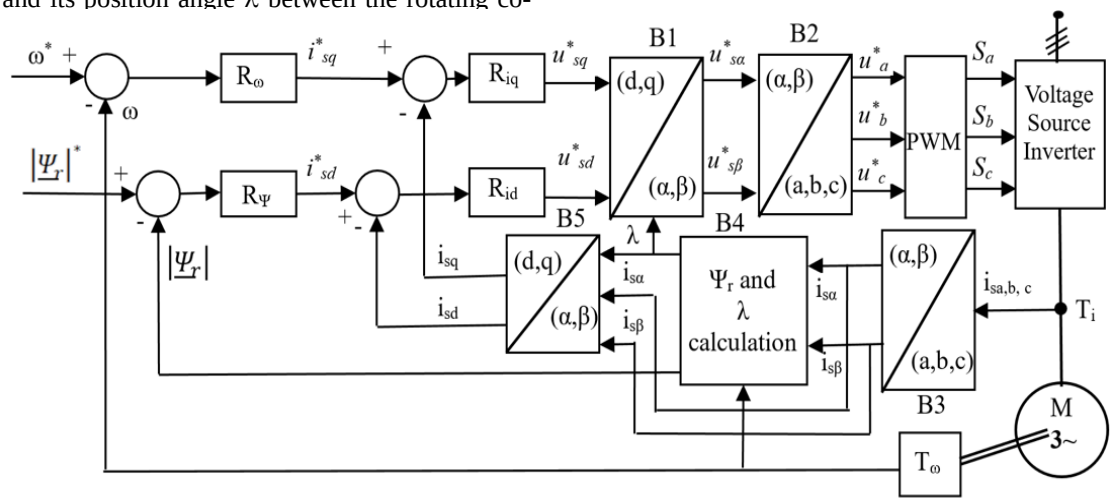

Fig. 1. Rotor flux and speed control scheme of a traction induction motor, based on rotor field-oriented control, with PWM modulator and voltage control.

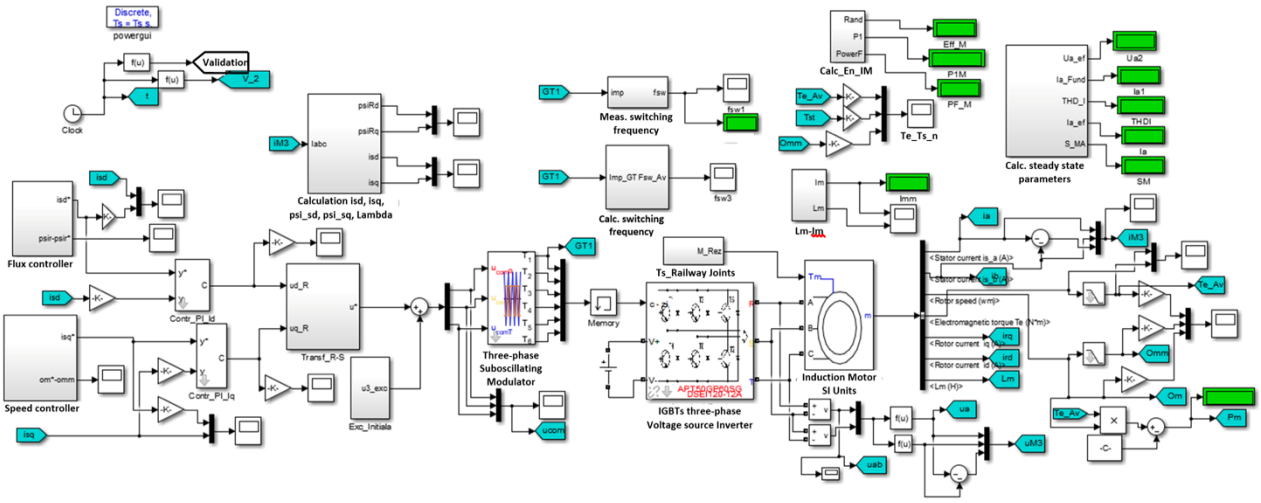

Fig. 2. Traction system Simulink model for testing the voltage control algorithm with sinusoidal PWM modulator and prescribing the rotor flux and speed.

In the control part, there are the rotor flux controller, the speed controller, the block for calculating the prescribed voltages on the motor phases from the stator current components in the rotor field oriented system "Transf_R-S", the three-phase sinusoidal modulator which also implements the voltage controllers for the three motor phases and the "Ts_Railway Joints" block which implements the resistant torque. There are also the current controllers and the three-phase sinusoidal modulator (block "Three-phase Suboscillating Modulator").

In the part of feedback control (block "Calculation isd, isq, psi_sd, psi_sq, Lambda), the main quantities are calculated by estimation. Also, the estimated magnetization inductance is used, which is obtained from the motor model based on the voltage – current dependence at idle conditions

There is a part for the calculation of steady-state energetic indicators (block "Calc. steady state parameters" which calculates and displays the phase voltage, the fundamental RMS current, total RMS current), harmonic distortion factor (*THD*) factor of the current through the motor and the apparent power).

Some quantities, such as the efficiency, power factor and active power related to the induction motor, are calculated and displayed in the block "Calc_En_IM". The three-axis oscilloscope "Te-Ts-n" displays the average torque, the resistant torque and the motor speed.

It should be noted that the speed controllers, as well as other calculation and display blocks, are validated by two signals obtained as functions of time, in the blocks at the top left of the figure. So, the speed and torque prescription takes place only after the motor is magnetized. Also, the rotor flux has the prescribed value.

A few more clarifications need to be made, as below.

The used controllers are of the proportional-integral (PI) type.

The rotor flux and the motor speed are prescribed as ramp signals.

For the limitation of the current, the outputs of the controllers are not limited to the input level (+10), but +5 V for the flux controller and +9.2 V for the speed controller.

In order to ensure the compatibility of the algorithm with the DSP system used on locomotives (Texas Instruments TMS320F28335), the Euler 1 integration method and the 40μs step (Ts) were used.

The sinusoidal PWM modulator operates with a switching frequency of 1 kHz.

In order to allow the overmodulation to achieve the nominal power at 100 Hz, the amplitude of the modulating (triangular) signal is 2.25 V, which also minimizes the current distortion and limits the noise.

IV. Performance of the Traction System

Table I and Table II illustrate the main parameters of the traction induction motor (a traction motor used in Romanian locomotives) and of the PI controllers. The value of the DC-voltage at the IGBT-based voltage source inverter input is 1800 V.

The motor start-up at constant resistant torque (T_s) and nominal rotor flux for speed below the rated value and diminished over the rated value, in case of three prescribed ramp speeds (248 rpm, three speed steps up to the nominal speed and maximal speed of 1983 rpm), are analyzed. Also, the periodic passage of wheels over rail joints was considered. For this, the load torque variation shown in Fig. 3 is considered, with the following parameters: $T_{sp} = 0.25 \cdot T_s$; $T_{sn} = -0.5 \cdot T_s$; $T_{mj} = 4$ s; $dt1 = 0.05 \cdot Tmj$; $dt0 = 0.1 \cdot dt1$; $dt2 = dt1$.

TABLE I.
Main Parameters of the Traction Induction Motor

V_N (V)	P_{2N} (kW)	f_{1N} (Hz)	I_N (A)	p	s_N	n_N (rpm)
1400	1150	62.5	576	3	0.0104	1237
T_N (N·m)	R_1 (Ω)	$L_{σ1}$ (mH)	R_2 (Ω)	$L_{σ2}$ (mH)	R_m (Ω)	L_{mN} (mH)
8877	0.021	0.288	0.012	0.275	89.38	9.46

TABLE II.
Parameters of the PI Controllers

$K_{pΩ}$	$T_{iΩ}$	$K_{pψ}$	$T_{iψ}$	K_{pid}	T_{iid}	K_{piq}	T_{iq}
100	0.004	10	0.04	0.3	0.1	0.15	0.6

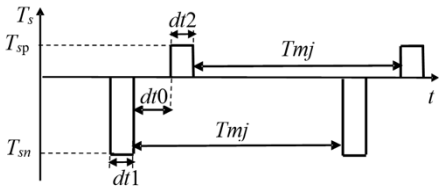

Fig. 3. Load torque during the passage of wheels over rail joints.

The evolution of several quantities (speed, rotor flux, electromagnetic torque, phase current, current and voltage components in the rotating reference frame, control and switching frequency) are analyzed. Also, different quantities specific to the steady-state operation and energetic indicators are given for each case study.

A. Case of Prescribed Speed of 248 rpm and T_s=T_N

When a low ramp speed of about 20% of the nominal speed (248 rpm) is prescribed at nominal resistant load, Fig. 4 – Fig. 14 illustrate the good response of the system.

It can be seen that the motor speed is very close to the prescribed value and, at the end of acceleration, the motor torque is very close to the load torque (Fig. 4). The speed is very little affected by the appearance of the rail joints, only ±2% (Fig. 4 and 5).

The rotor flux also faithfully follows the prescribed value (Fig. 6).

The i_{sd} current has a maximum for fast motor magnetization (Fig. 7), then become constant. The active current (i_{sq}) follows the evolution of the torque (Fig. 8). There are some current increases (about 1100 A, but maxim admissible value is 1200 A) related to the appearance of the rail joints (Fig. 9).

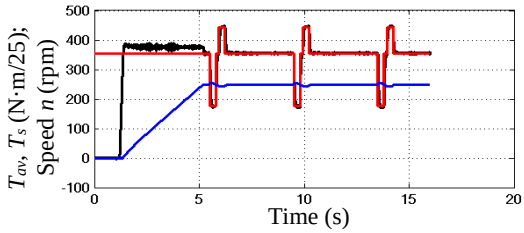

Fig. 4. Time evolution of the average torque (black), resistant torque (red) and speed (blue) at the prescribed speed of 248 rpm during the whole process.

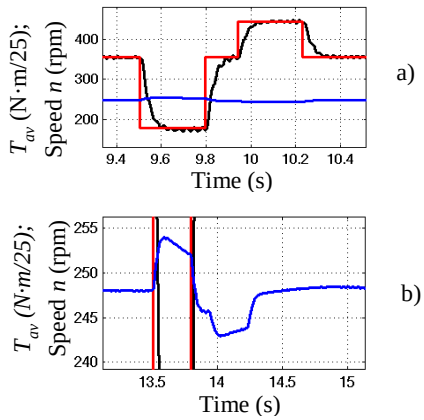

Fig. 5. Details in fig a) and b) regarding the evolution of the average torque (black), resistant torque (red) and speed (blue) during the passage of a wheel over a rail joint at the prescribed speed of 248 rpm.

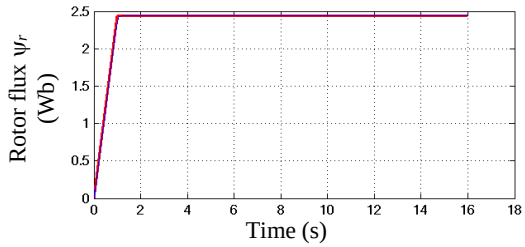

Fig. 6. Rotor flux (prescribed – in red and actual – in black) at the prescribed speed of 248 rpm.

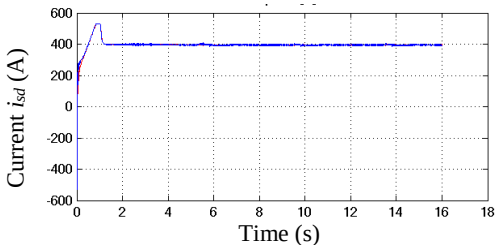

Fig. 7. d-axis stator current (prescribed – in red and actual – in black) at the prescribed speed of 248 rpm.

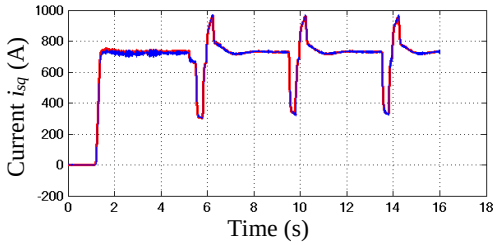

Fig. 8. q-axis stator current (prescribed – in red and actual – in black) at the prescribed speed of 248 rpm.

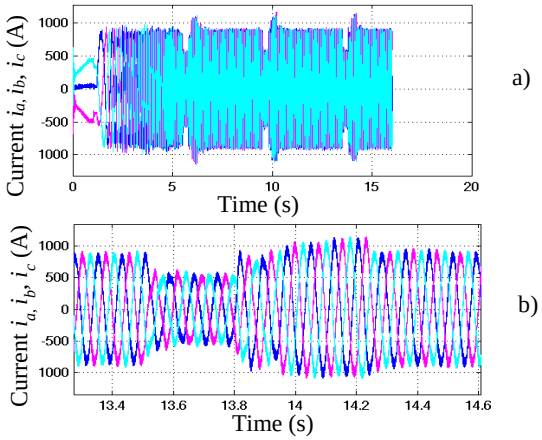

Fig. 9. Stator currents on the three phases at the prescribed speed of 248 rpm: a) during the whole process; b) detail on an interval of 1.2 s.

The resulted d and q components of the stator voltage are illustrated in Fig. 10 and Fig. 11, and show that there are low influences between them. As shown in Fig. 12 and Fig. 13, the switching frequency is variable, but it average value does not exceed 1 kHz. Fig. 13 shows the increase of the stator voltage frequency up to the value of about 13 Hz.

Table III synthesizes the dynamic performance of the system. δT and δn are the torque and speed variations. Table IV summarizes the steady-state performance. A low power factor (*PF*) of 37 % and a relatively low value of the current harmonic distortion (THD_I) of 7 % are highlighted.

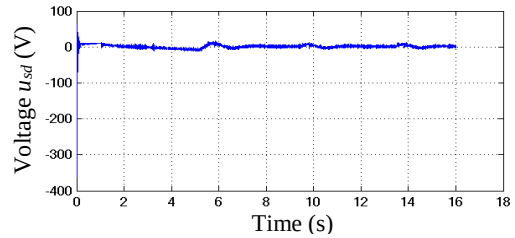

Fig. 10. d-axis component of the stator voltage at the prescribed speed of 248 rpm.

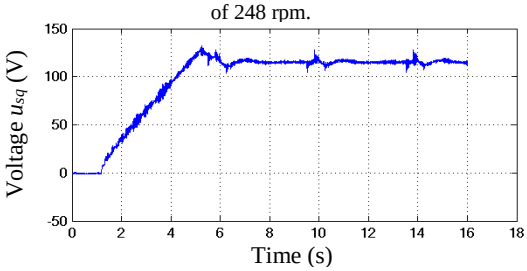

Fig. 11. q-axis component of the stator voltage at the prescribed speed of 248 rpm.

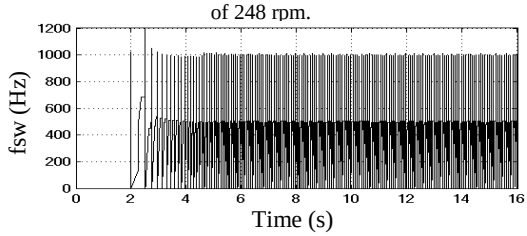

Fig. 12. Evolution over time of the average switching frequency at the prescribed speed of 248 rpm.

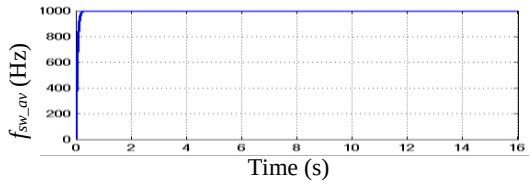

Fig. 13. The average switching frequency (averaged over 10 ms), at the prescribed speed of 248 rpm.

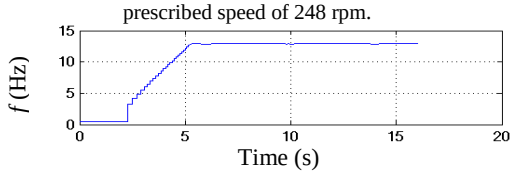

Fig. 14. The control frequency, at the prescribed speed of 248 rpm.

TABLE III.
DYNAMIC PERFORMANCE AT THE PRESCRIBED SPEED OF 248 RPM

T_{s-} (%)	T_{s+} (%)	δT (%)	δn_+ (%)	δn_- (%)	$I_{max.\_acc.}$ (A)	$I_{max.\_steady-st.}$ (A)	f_{sw_max} (kHz)
-50	25	100	2	2	1100	1160	1

TABLE IV.
STEADY-STATE PERFORMANCE AT THE PRESCRIBED SPEED OF 248 RPM

V (V)	I [A]	$I_{magn.}$ (A)	P_1 (kW)	P_m (kW)	S (kVA)	PF (%)	η (%)	THD_I (%)
398	596	209	260	225	701	37	86.73	7

B. Prescribing Speed up to Nominal Value in Three Steps and Braking in Two Steps

For prescribing speed step by step up to the nominal value, also with brake, the waveforms of the main quantities are illustrated in Fig. 15 - Fig. 24. (the passage of wheels over the rail joints is neglected).

First, new information is offered by d-axis stator current (Fig. 15) that, after 10 seconds decreases, although the rotor flux remains constant (Fig. 16). After the brake control is given, the current increases and reach the rated value. The speed follows the prescribed values both during the accelerating and braking regimes (Fig. 17). The q-axis stator current (Fig. 18) has the constant values in steady-state, increases in the time of acceleration and decreases in braking time. It is significant that, it does not have negative values, similar to the torque (Fig. 19). It means that the motor does not operate in braking regime and the decreasing of the speed is caused by the resistant torque only.

The phase currents of the motor are under 1000 A on the first two steps and exceed a little 1000 A at the nominal speed (Fig. 20). The average switching frequency is 1 kHz for speed under 1000 rpm, but decreases to 400 Hz when the speed is over 1000 rpm (Fig. 21).

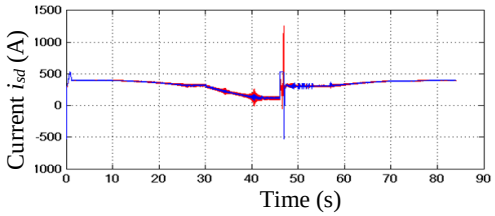

Fig. 15. Time evolution of stator current along the d-axis (prescribed in blue and actual in red) when speed is stepped up to nominal speed and braking.

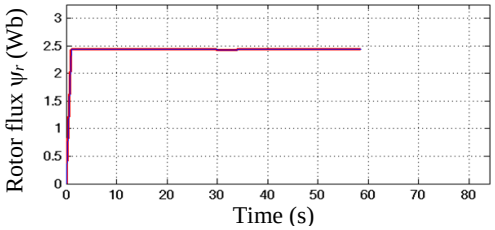

Fig. 16. The time evolution of the rotor flux (prescribed and actual in red) from speed prescription in steps up to nominal speed and braking.

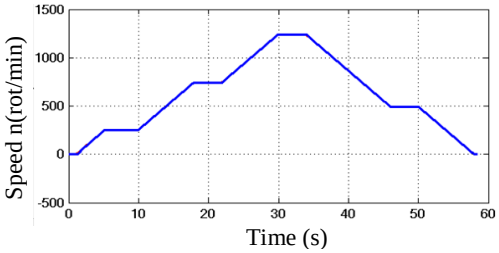

Fig. 17. Speed evolution over time (prescribed in blue and actual in red), in the case of speed prescription in gears up to nominal speed and braking.

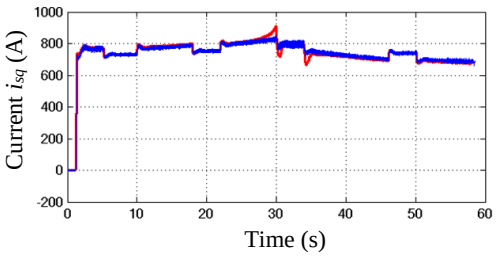

Fig. 18. The time evolution of the q-axis component of the stator current (prescribed in blue and actual in red), when prescribing the speed in steps up to rated speed and braking.

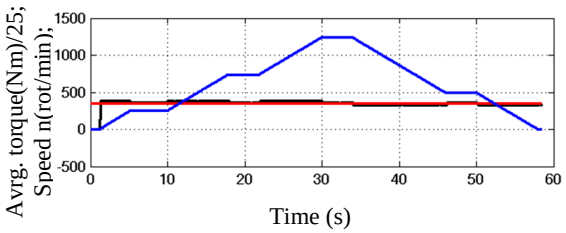

Fig. 19. Evolution over time of the average torque (black) and speed (blue), when prescribing the speed in gears up to nominal speed and braking.

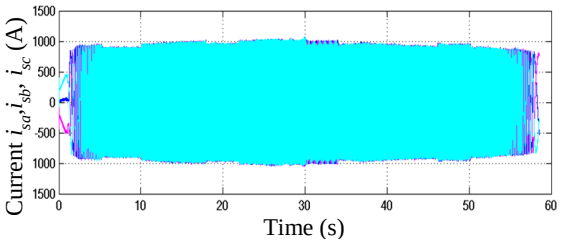

Fig. 20. Time evolution of the currents on the 3 phases, from speed prescription in steps up to nominal speed and braking.

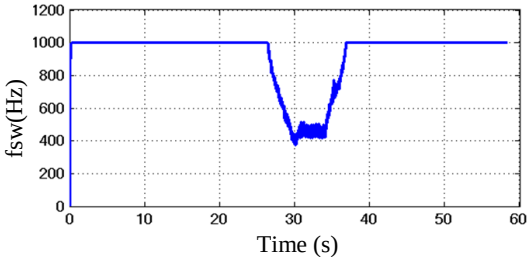

Fig. 21. The time evolution of the switching frequency averaged over 10 ms, when prescribing the speed in steps up to nominal speed and braking.

The time evolution of the stator voltage on the component along the d-axis is similar to that of the stator current of the same axis (Fig. 22), because the voltage determines the current.

Because the rotor flux is constant, the time evolution of the stator voltage component on the q-axis is similar to that of the torque (Fig. 23).

The form of the cosin of the rotor flux position angle (Fig. 24-a) proves a good orientation of the calculation system. The control frequency follows the speed as form (Fig. 24-b). It means that the slip is very low.

C. Case of Prescribed Speed of 1983 rpm and T_s=0.625·T_N

For the highest speed (1983 rpm), the waveforms of the main quantities are illustrated in Fig. 25 - Fig. 37 and the performance summary is presented in Table V and Table VI. The resistant torque is diminished so that, over the nominal speed, the power to be at nominal value.

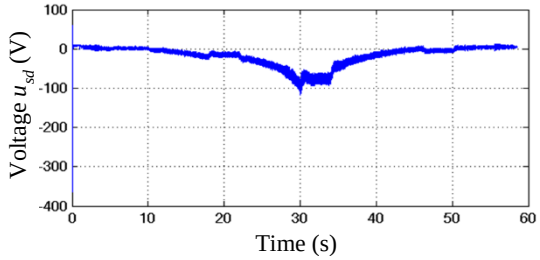

Fig. 22. The time evolution of the component along the d-axis of the stator voltage, in the case of stepped speed prescription up to rated speed and braking.

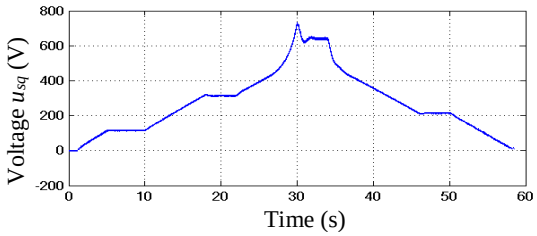

Fig. 23. The time evolution of the component along the q-axis of the stator voltage, in the case of stepped speed prescription up to rated speed and braking.

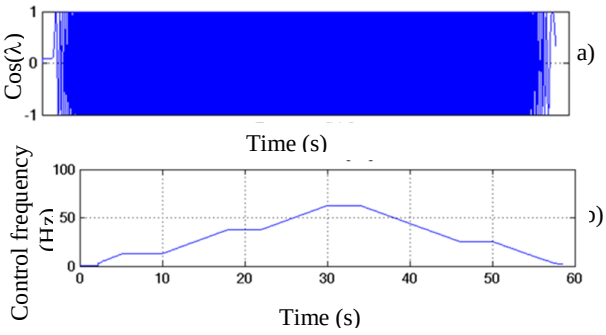

Fig. 24. The evolution over time of: a) the cosine of the angle of the rotating system; b) the control frequency, in the case of prescribing the speed in steps up to nominal speed and braking.

The prescribed speed is followed very well by the real speed and the effects of passing the joints are diminished (Fig. 25). The details from Fig. 26 and Fig. 27 underline some aspects. Thus, the motor torque does not follow the resistant torque, and its variation represents less than 50% of resistant torque variation. The total and the d-axis rotor flux are diminished over nominal speed and have a hyperbolic evolution (Fig. 28 and Fig. 29). Also, the q-axis rotor flux is null because the calculation system is well oriented (Fig. 29). The d-axis stator current decreases when the speed increases, especially over of the nominal speed (Fig. 30). At nominal speed, the d-axis stator current becomes near zero. The q-axis stator current increases when the speed exceeds the nominal value and magnetic flux decreases (Fig. 31). The real current does not have variations when the wheels passing over the joints.

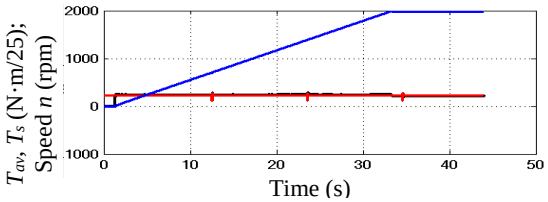

Fig. 25. Time evolution of the average torque (black), resistant torque (red) and speed (blue) at the prescribed speed of 1983 rpm.

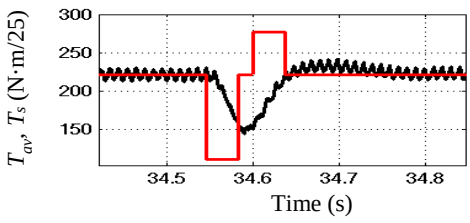

Fig. 26. Detail regarding the evolution of the average torque (black) and resistant torque (red) during the passage of a wheel over a rail joint at the prescribed speed of 1983 rpm.

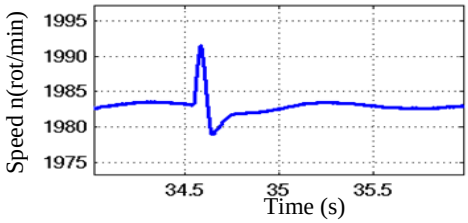

Fig. 27. Detail regarding the evolution of the speed during the passage of a wheel over a rail joint at the prescribed speed of 1983 rpm.

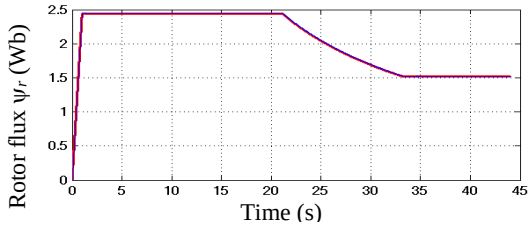

Fig. 28. Rotor flux (prescribed – in red and actual – in black) at the prescribed speed of 1983 rpm.

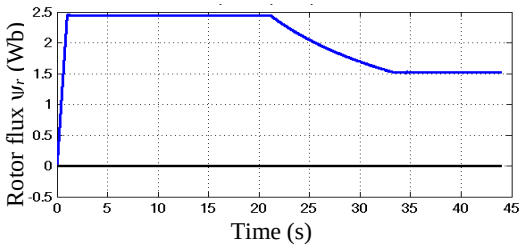

Fig. 29. Components of the rotor flux on the two axes (d-axis rotor flux – in blue and q-axis rotor flux – in black) at the prescribed speed of 1983 rpm.

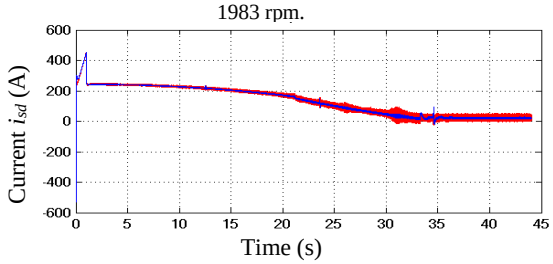

Fig. 30. d-axis stator current (prescribed – in red and actual – in black) at the prescribed speed of 1983 rpm.

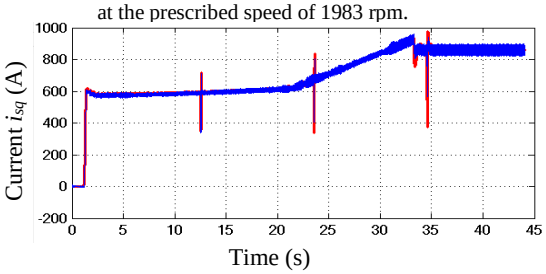

Fig. 31. q-axis stator current (prescribed – in red and actual – in blue) at the prescribed speed of 1983 rpm.

This aspect is showed better by phases current (Fig. 32). There is a little diminution of the current when the prescribed speed is obtained and the acceleration torque disappears. The d-axis component of the stator voltage evolves similarly to that of the corresponding current (Fig. 33). It should be noted that the final values are negative (about – 250 V).

Also, the q-axis component of the stator voltage evolves similarly to that of the active current (Fig. 34). After the nominal value of the supply voltage is obtained, the switching frequency decreases because the phase voltage is more little modulated (Fig. 35). The control frequency increases to 100 Hz, larger of 1.6 time from the nominal value (Fig. 36).

The magnetizing inductance and current (Fig. 37), shows that the inductance increases a little although the current decreases from 180 A to 100 A. This means that the motor is not saturated.

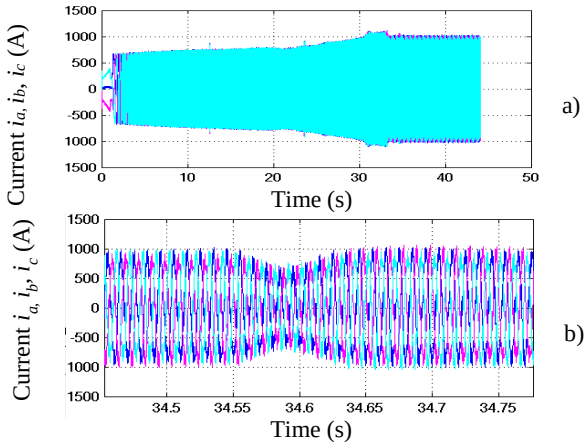

Fig. 32. Stator currents on the three phases at the prescribed speed of 1983 rpm: a) during the whole process; b) detail during the passage of a wheel over a rail joint.

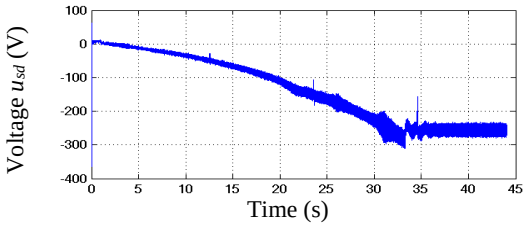

Fig. 33. d-axis component of the stator voltage at the prescribed speed of 1983 rpm.

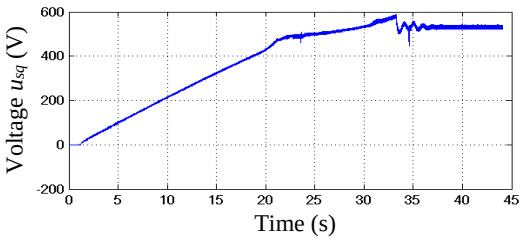

Fig. 34. q-axis component of the stator voltage at the prescribed speed of 1983 rpm.

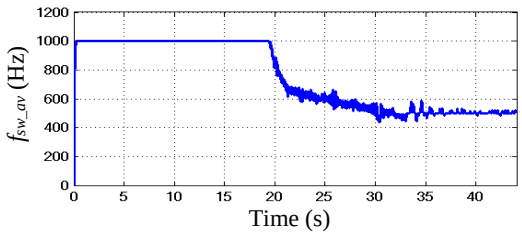

Fig. 35. The average switching frequency (averaged over 10 ms), at the prescribed speed of 1983 rpm.

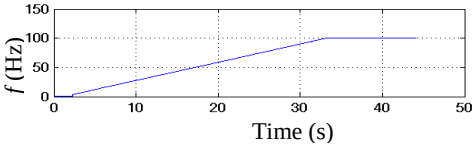

Fig. 36. The control frequency, at the prescribed speed of 1983 rpm.

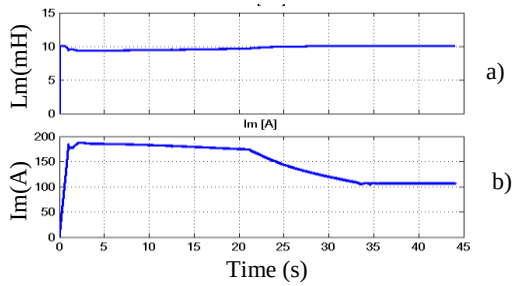

Fig. 37. Time evolution of: a) magnetizing inductance; b) magnetizing current, at the prescribed speed of 1983 rpm.

V. Possibility Of Implementation

The d-axis stator current decreases with increasing speed although the rotor flux is constant. This aspect does not respect the physical phenomenon and the operating equations of the induction motor in the rotor flux oriented system [12]:

$$0 = R_r i_{rd} + \frac{d}{dt}\Psi_{rd}; \tag{6}$$

$$\Psi_{rd} = L_r i_{rd} + L_m i_{sd}. \tag{7}$$

Equations (6) and (7) show that, if ψ_{rd}=constant, two very important aspects can highlight the correctness of the algorithm: $i_{rd} = 0$; $i_{sd} = \psi_{rd}/L_m$ = constant, because ψ_{rd} = constant also involves L_m = constant.

It is found that, even at very high speed, the performance is good (Tab. V and VI).

TABLE V.
Dynamic Performance at the Prescribed Speed of 1983 rpm

T_{s-} (%)	T_{s+} (%)	δT (%)	δn_+ (%)	δn_- (%)	$I_{max.\_acc.}$ (A)	$I_{max.\_steady-st.}$ (A)	f_{sw_max} (kHz)
-50	25	75	0.5	0.23	1100	1025	1

TABLE VI.
Steady-State Performance at the Prescribed Speed of 1983 rpm

V (V)	I [A]	$I_{magn.}$ (A)	P_1 (kW)	P_m (kW)	S (kVA)	PF (%)	η (%)	THD_I (%)
828	614	107	1184	1124	1526	77.6	94.95	17.23

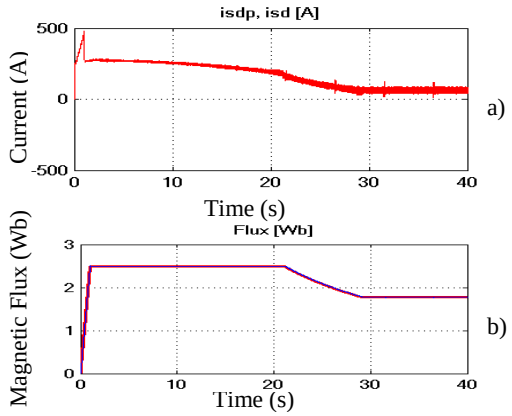

Fig. 38. Time evolution of: a) current; b) magnetic flux, at the prescribed speed of 1983 rpm.

It is appreciated that the appearance is determined by the calculation error, especially when calculating the position angle of the rotor flux. There are two ways to reduce calculation errors: using a smaller integration step and using an integration method of order 2 or higher. The first modality was verified for Ts=5μs (Fig. 38). But, this sampling period can't be used for real-time implementation, because it is too small.

In same time, the dSPACE 1103 prototyping board, used for the code generation operates by first order integration method, as the used processor too. Consequently, the research activity will continue with the development, implementation and testing of a calculation sequence that details the 2nd order integration. Only then, will tests be carried out on the physical model.

VI. Conclusions

Following the analysis of the energetic and dynamic performance of the traction system with rotor flux-oriented control in the acceleration, steady state and braking regimes, few aspects can be highlighted.

The evolution of all quantities, excepting d-axis stator current, respects the physical phenomenon and the operating equations of the motor.

The current absorbed by the motor is higher than the nominal value, by about 3% at the low prescribed speed and by about 10% at the highest prescribed speed.

The power factor is significantly lower than in sinusoidal supply conditions and increases with speed. The efficiency has very good values (86.73 % to 97.3 %). *THDI* has a low value (7%) at low speed and increases at high speed (17.23%).

The maximum average switching frequency is below the maximum allowed value of 1100 Hz.

When passing over the rail joints, the torque accurately follows the variations of the resistant torque, so the speed variations are very small. In conclusion, the rotor flux-oriented control leads to good performance when applied to the traction induction motor.

Acknowledgment

Source of research funding in this article: Research program financed by the University of Craiova.

Contribution of authors:

First author – 50%

First coauthor – 30%

Second coauthor – 10%

Third coauthor – 10%

Received on September 7, 2024

Editorial Approval on December 2, 2024

References

[1] F. Blaschke, "The principle of field orientation as applied to the new transvector closed loop control system for rotating field machines," *Siemens Rev*, vol. 39, no. 5, pp. 217–220, May 1972.

[2] B. Robyns, B. François, P. Degobert, and J.P. Hautier, *Vector Control of Induction Machines*, Springer, 2012.

[3] N.P. Quang and J.-A. Dittrich, *Vector Control of Three-Phase AC Machines*, Springer, 2015.

[4] S. Peresada, Y. Nikonenko and S. Kovbasa, "Field-weakening methods for torque-flux direct field-oriented control of induction motors," *2022 IEEE 8th International Conference on Energy Smart Systems (ESS)*, Kyiv, Ukraine, 2022, pp. 292-296.

[5] M. Popescu, A. Bitoleanu and C. V. Suru, "Influence of locomotive wheels slipping on a traction system with rotor flux-oriented

control and hysteresis current controllers," *2023 13th International Symposium on Advanced Topics in Electrical Engineering (ATEE)*, Bucharest, Romania, 2023, pp. 1-6.

[6] P. Xie, G. Li, F. Xie, C. Hu and X. Qi, "Research on field-weakening control of induction motor based on torque current component of the voltage closed-loop," *2015 IEEE 10th Conference on Industrial Electronics and Applications (ICIEA)*, Auckland, New Zealand, 2015, pp. 1618-1621.

[7] F. Briz, A. Diez, M. Degner, and R. Lorenz, "Current and flux regulation in field-weakening operation [of induction motors]," *IEEE Trans. On Industry Applications*, vol. 37, no. 1, pp. 42-50, 2001.

[8] S. K. Kakodia and G. Dynamina, "A Comparative study of DFOC and IFOC for IM drive, " *2020 First IEEE International Conference on Measurement, Instrumentation, Control and Automation (ICMICA)*, Kurukshetra, India, 2020, pp. 1-5.

[9] I. Ferdiansyah, S. D. Nugraha, O. A. Qudsi, L. P. S. Raharja, D. S. Yanaratri and R. P. Eviningsih, "Implementation of FPGP-PID for dynamic speed control of three phase induction motor based on IFOC," *2019 6th International Conference on Instrumentation, Control, and Automation (ICA)*, Bandung, Indonesia, 2019, pp. 24-29.

[10] H. Kim, Y. Han and K. Lee, "Improved Q-MRAS based online rotor time constant compensation for IFOC induction motor drives," *2023 IEEE Applied Power Electronics Conference and Exposition (APEC)*, Orlando, FL, USA, 2023, pp. 1-6.

[11] S. Yadav and A. K. Mishra, "Performance evaluation in IFOC induction motor drive with various PWM techniques," *2020 International Conference on Electrical and Electronics Engineering (ICE3)*, Gorakhpur, India, 2020, pp. 65-70.

[12] M. Popescu, A. Bitoleanu and C. V. Suru, "Performance of traction system with induction motor and rotor field orientation by voltage control", *2022 22nd International Symposium on Electrical Apparatus and Technologies (SIELA)*, Bourgas, Bulgaria, 2022, pp. 1-4.

[13] M. Popescu, A. Bitoleanu and C. V. Suru, "Estimation of the rotor flux in the traction systems with induction motors and field-oriented control," *2023 International Conference on Electromechanical and Energy Systems (SIELMEN)*, Craiova, Romania, 2023, pp. 1-6.

[14] A. Bitoleanu, M. Popescu and V. Suru, "Experimental evaluation of rotor field orientation control and hysteresis controller for induction traction motor," *2021 12th International Symposium on Advanced Topics in Electrical Engineering*, Bucharest, Romania, 2021, pp. 1-6.

[15] C. V. Suru, M. Popescu and M. Linca, "Implementation of rotor field orientation by voltage control on dSPACE system," *2022 22nd International Symposium on Electrical Apparatus and Technologies (SIELA)*, Bourgas, Bulgaria, 2022, pp. 1-4.

[16] M. Popescu and A. Bitoleanu, "New achievements in the rotor field -oriented control for autonomous locomotives. Part 1: System synthesis and theoretical investigations," *The 7th International Symposium on Electrical and Electronics Engineering (ISEEE 2021)*, October 28-30, 2021 Galați, Romania, pp. 1–6.

[17] R. Garg, P. Mahajan, N. Gupta and H. Saroa, "A comparative study between field oriented control and direct torque control of AC traction motor," *International Conference on Recent Advances and Innovations in Engineering (ICRAIE-2014)*, Jaipur, India, 2014, pp. 1-6.

[18] V. Burenin, J. Zarembo, G. Kobenkins and O. Krievs, "Implementation of hybrid PWM with smooth transitions between modulation modes for railway traction field-oriented control system," *2023 IEEE 64th International Scientific Conference on Power and Electrical Engineering of Riga Technical University (RTUCON)*, Riga, Latvia, 2023, pp. 1-7.

[19] M. Popescu and A. Bitoleanu, "Diagnosis of passing over railway joints and reducing the effects in modern traction systems," *2023 IEEE 14th International Symposium on Diagnostics for Electrical Machines, Power Electronics and Drives*, Chania, Greece, 2023, pp. 436-442.

[20] T. Mătușa, M. Popescu, A. Bitoleanu and C. V. Suru, "Behavior of a Traction Induction Motor with Rotor Flux-Oriented Control," *2024 International Conference on Applied and Theoretical Electricity (ICATE)*, Craiova, Romania, 2024, pp. 1-6.